MAGNETISM AND (HIGH-TEMPERATURE) SUPERCONDUCTIVITY

Joël Mesot
Laboratory for Neutron Scattering
Institut Paul Scherrer & ETH Zurich
CH-5232 Villigen PSI
Switzerland

Inelastic neutron scattering has revealed the existence of strong magnetic fluctuations in high-temperature cuprate superconductors. While in the undoped parent compound excitations, originating from the (π,π) antiferromagnetic wave vector, can be explained by simple spin-wave theory, the situation is more complex for the doped materials. Indeed the magnetic excitations renormalize in a spectacular way through the superconducting critical temperature T_c. This raises the question of the role played by magnetism for superconductivity in the cuprates and in particular, of its connection to the one-electron spectral function? Finally, small angle neutron scattering investigations of the vortex lattice structure in the mixed phase of HTSC are also introduced.

1. Introduction

The phenomenon of superconductivity (SC) was first discovered in 1911 by Kamerlingh-Onnes who observed a sudden drop of the resistance in Mercury below a critical temperature T_c of 4.2 K (see Figure 1). Onnes furthermore observed that superconductivity can be destroyed by the application of a large enough current J or magnetic field H.

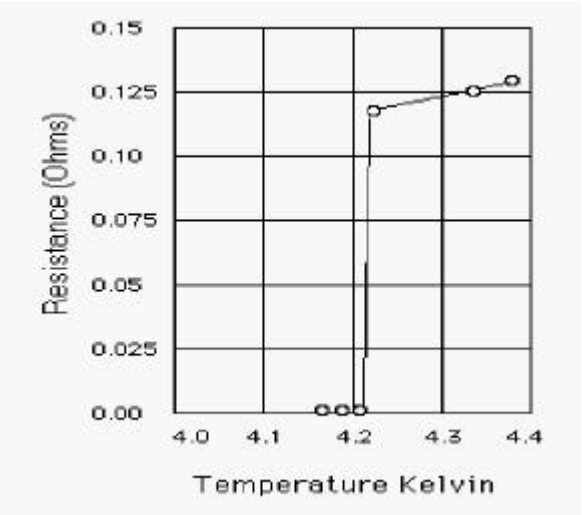

Figure 1: Resistance of a Mercury wire as measured by Onnes.

Later (1933) Meissner and Ochsenfeld discovered that a superconductor behaves like a perfect diamagnet: under the application of an external magnetic field, the induction B vanishes inside the superconductor: this is the so-called Meissner effect.

A complete theoretical understanding of superconductivity in simple metals was only achieved more than 40 years after its discovery. In 1934 Gorter and Casimir developed a first thermodynamical approach of SC and in 1935 London could explain the Meissner effect. A more complete phenomenological theory was elaborated by Ginzburg and Landau in 1950. This theory uses a Gauge invariance and introduces the concept of order-parameter, that allows describing the system in the vicinity of the critical temperature. Abrikosov[1] in 1957 anticipated that for Type-II superconductors, where the magnetic flux can penetrate into the sample in form of quantized vortices, a vortex lattice can be formed. His prediction was verified experimentally 10 years later. Examples of the determination of the vortex lattice by means of neutron scattering will be given in Section 4.

The path toward a microscopic theory of SC was guided by the observation that T_c depends on the mass M of the atom: $T_c \sim M^{-\alpha}$. In 1950 Fröhlich proposed the electron-phonon interaction as the mechanism responsible for superconductivity, which provides an exponent α=0.5. As can be seen in table 1, this is true for most simple metals, but there are some examples showing strong deviations from 1/2. A quantitative description of SC was realized by Bardeen Cooper and Schrieffer[2] (BCS) in 1957. This non-perturbative theory describes SC in terms of Cooper-pairs bound by a weak (electron-phonon) interaction. As a result, a SC-gap opens in the electronic density-of-state and a simple relation was established between the zero-temperature SC-gap value ? and T_c: $2?(T=0) \sim 3.5\ k_B T_c$. Notice that in such models the gap function is assumed to show no or little k-dependence.

Table 1: measured coefficients α of the isotopic effect $T_c \sim M^{-\alpha}$

	α		α
Hg	0.50±0.03	Cd	0.50±0.10
Tl	0.50±0.10	Mo	0.33±0.05
Sn	0.47±0.02	Ru	0.00±0.10
Pb	0.48±0.01	Os	0.20±0.05

This theory was such a success that J. M. Ziman wrote in his introduction to SC [3]: “SC was long considered the most extraordinary and mysterious of the properties of metals; but the theory of Bardeen, Cooper and Schrieffer –the BCS theory- has explained so much that we can say that we now understand the superconducting state almost as well as we do the normal ‘state’.”

In 1986 Tilley and Tilley in their book on Superconductivity and Superfluidity[4] wrote some general experimental facts about superconductors:

A) Only metals become superconductors
B) T_c is always below about 20 K (see Figure 2)

C) Good conductors are not the best superconductors
D) Magnetic metals do not superconduct

We shall see in the following that these conclusions have been strongly questioned since then.

2.1 The high-temperature superconductivity (HTSC) revolution

The state of the research on SC was revolutionized in 1986[5], when Georg Bednorz and Karl Alex Müller from IBM Rüschlikon, Switzerland, demonstrated the existence of superconductivity in the perovskites $La_{2-x}(Ba,Sr)_xCuO_4$ (La214), x<1). Soon after new materials ($YBa_2Cu_3O_{7-\delta}$ (Y123), $Bi_2Sr_2CaCu_2O_{8+\delta}$ (Bi2212) (δ<1)) have been discovered with T_c values breaking the temperature of liquefaction of Nitrogen. It was realized that the phonon-interaction alone would not be sufficient to explain the high critical temperatures observed in the cuprates and various competing theoretical models have been proposed. In particular magnetism was very early recognized as one of the key element to understand HTSC[6].

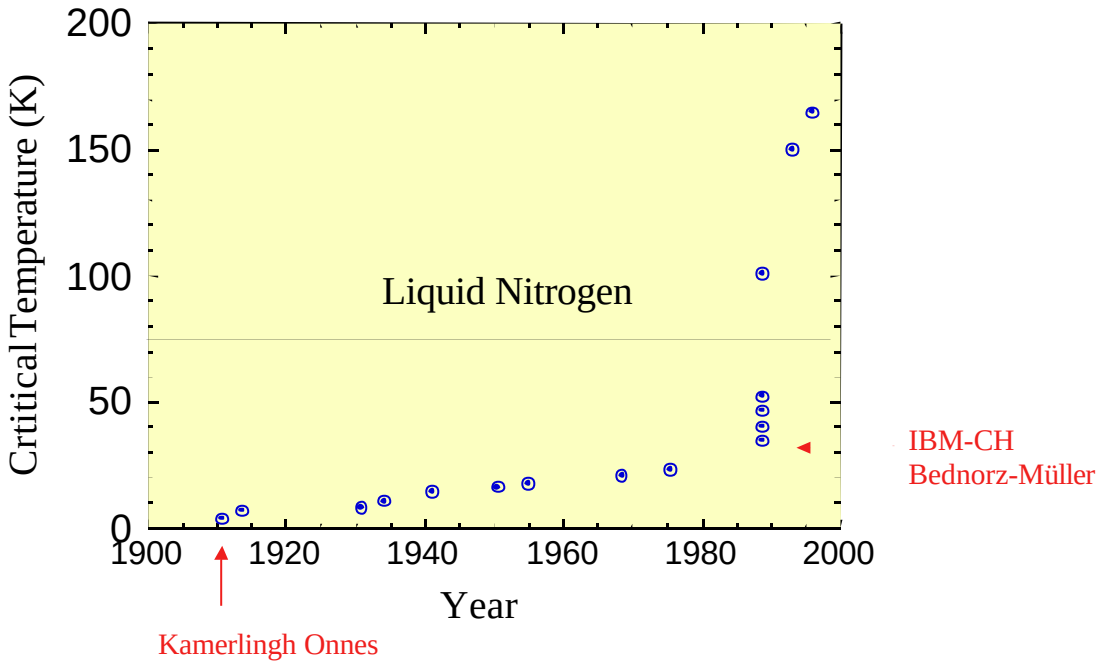

Figure 2: Evolution of T_c throughout the years. Notice the change of slopes after the discovery, in 1986, of SC in Cu-perovskite materials.

2.2 Extraordinary properties of HTSC

These materials are doped insulators (La_2CuO_4 is a Mott insulator) with a very anisotropic layered structure (see Figure 3) composed of CuO_2 layers alternating with so-called reservoir layers (see Figure 3). By modifying the reservoir-layers one can control both the doping level of the CuO_2 planes and T_c.

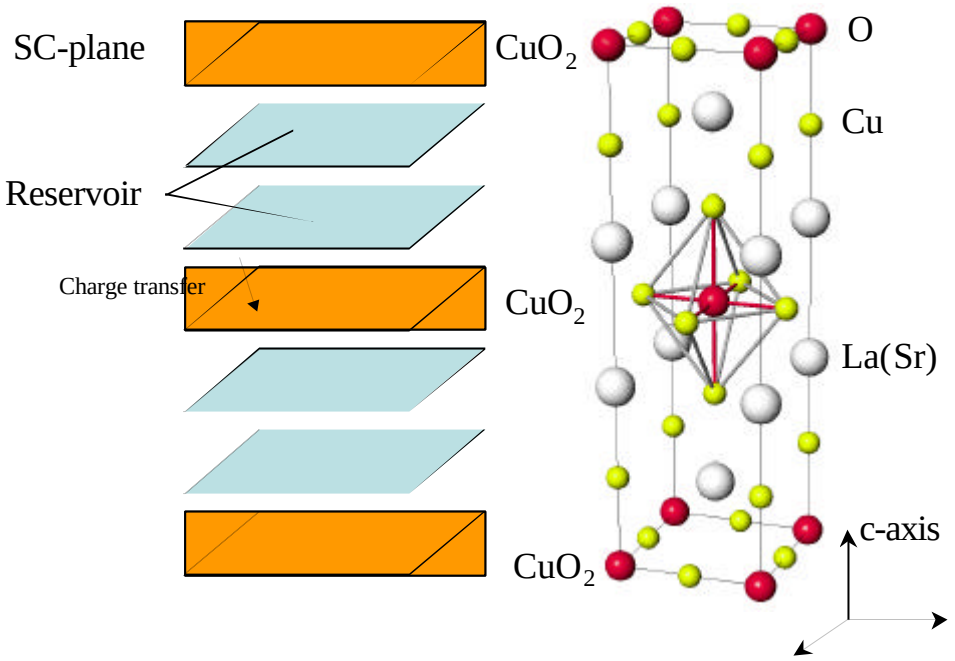

Figure 3: Layered structure of the $La_{2-x}Sr_xCuO_{4+\delta}$. By modifying the chemical composition of the reservoir layers, one can control the doping level in the SC-planes.

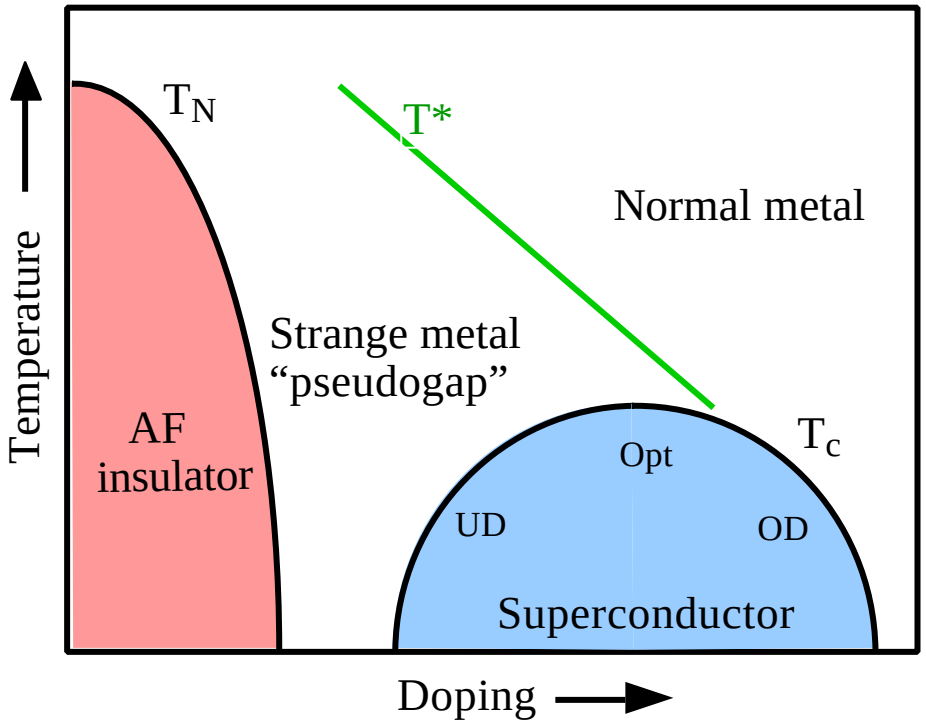

Figure 4: Sketch of the phase diagram of cuprates

The undoped system is antiferromagnetic (AF) and insulating (Figure 4). At small doping, the Néel temperature T_N decreases rapidly and vanishes. The system enters then a spin-glass phase. Upon further doping superconductivity appears below a critical temperature T_c, but the system behaves like a strange metal (underdoped (UD) regime). T_c reaches then an optimum (Opt) and decreases again (overdoped (OD) regime).
The proximity of the AF and SC naturally raises the question of the importance of magnetism for the existence of SC. One prediction of models involving magnetism was the existence of a superconducting gap parameter that would change sign upon 90 degrees rotation (so called d-wave SC gap function). Indeed, a SC gap function with nodes (see Figure 5) has been clearly identified by means of angle resolved photoemission spectroscopy[7] (ARPES) and phase sensitive[8] experiments. We shall see that this finding is crucial for the understanding of the neutron data presented in the following Sections. HTSC also differ from low-T_c materials by the observation, in the UD state, of the existence of a pseudogap[9] well above T_c, both in the charge and spin sectors. This pseudogap closes at a temperature T* that is increasing with decreasing doping (see green line in Figure 4) and the ratio of $?_{max}(T=0)/T_c$ increases with underdoping.

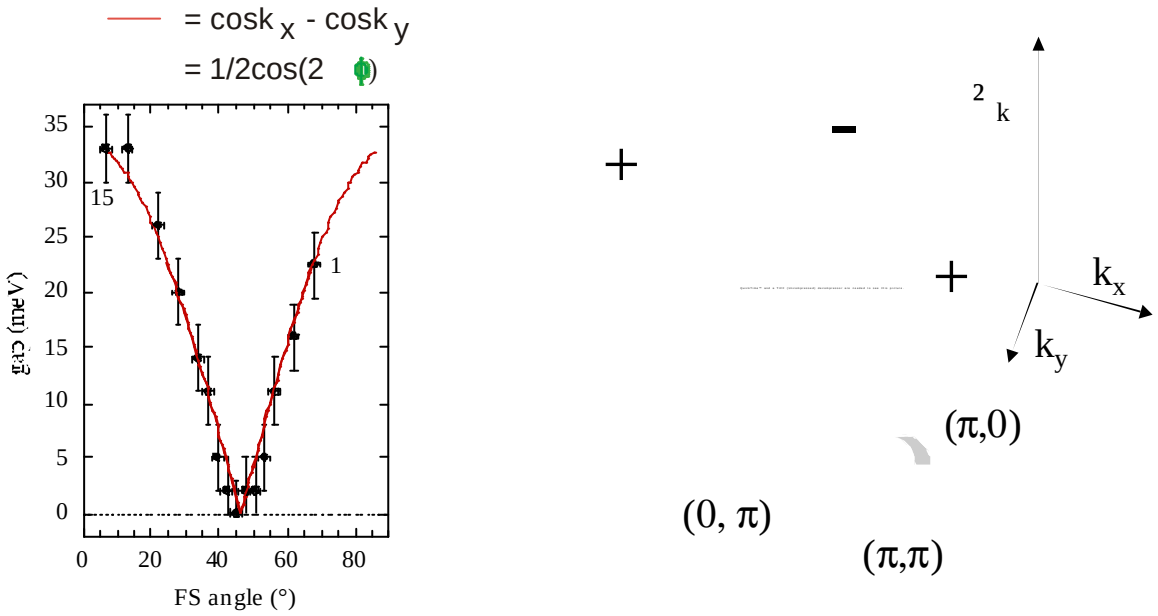

Figure 5, left: ARPES determination[7] of the angle ϕ dependence of the SC-gap. Right: reconstruction of the Fermi surface and gap function as determined from ARPES[10]. The + and - signs indicate the sign change expected for a d-wave gap function upon 90 deg. rotation. The angle ϕ on the Fermi surface (FS) is defined by the grey arrow.

3. Magnetism in cuprates

3.1 Inelastic neutron scattering

Inelastic neutron scattering allows a direct measurement of the magnetic scattering function $S_{\alpha\beta}(\mathbf{Q},\omega)$: the Fourier transform both in time and space of the spin-spin correlation function (see lecture by H. Schober, this school). $S_{\alpha\beta}(\mathbf{Q},\omega)$ is in turn related, through the fluctuation-dissipation theorem, to the imaginary part of the dynamical generalized spin susceptibility c''_{ab} via:

$$S_{ab}(\mathbf{Q},w) = \frac{1+n(w)}{p\left(gm_B\right)^2} c''_{ab}(\mathbf{Q},w) \qquad (1)$$

The measured susceptibility can then be compared to the one calculated using various microscopic models. An example of such a comparison is given in Section 3.4. Both conventional triple-axis (see examples below) and time-of-flight[11] spectrometers have been used to measure the magnetic excitations in HTSC.

3.2 Undoped cuprates

3.2.1 Magnetic structure

In the undoped case, the Cu^{2+} atoms ($3d^9$, S=1/2) in the CuO_2 planes order antiferromagnetically with a propagation vector (1/2, 1/2, 0) as was determined for La124 and Y123 from both powder[12] and single crystal studies[13]. While in La214[14], the moment direction is along the (1,1,0) direction, a study of the evolution of the magnetic intensity as a function of magnetic field has shown that in Y123 the moment direction is along the (100) direction, implying a small in-plane anisotropy[15]. The value of the ordered moment appears to be strongly reduced with respect to the 1 μB corresponding to S=1/2. Experiments have yielded ordered moments in the range 0.3-0.6 μB and several possible origins have been considered to explain this reduction: g factor of Cu^{2+}; covalency effects due to hybridisation of the copper and oxygen atoms; quantum fluctuations expected in low-dimensional antiferromagnet with small spin.[16]

3.2.2 Spin waves in a square lattice antiferromagnet

The coupling between neighbouring spins in a square lattice antiferromagnet is described by the Heisenberg Hamiltonian:

$$\mathrm{H} = \sum_{\langle ij \rangle} \mathrm{J}\mathbf{S}_i\mathbf{S}_j \qquad (2)$$

where J is the nearest-neighbor superexchange coupling constant (Figure 6A).

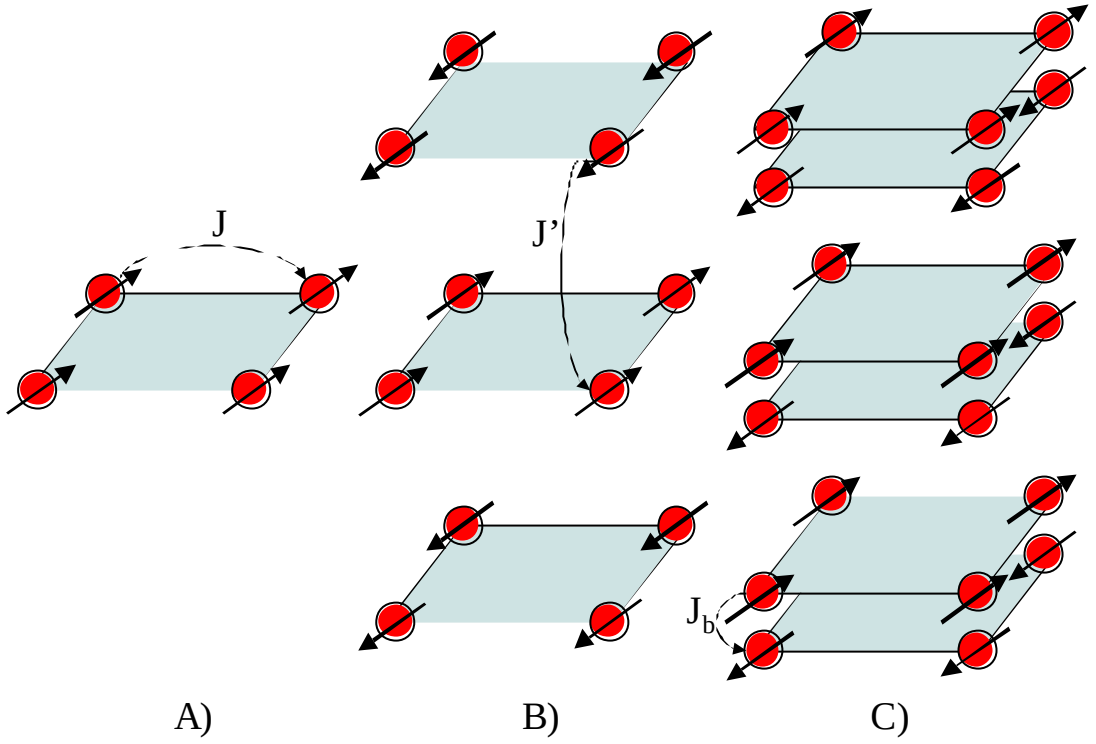

Figure 6: A) Simple square AF. B) Magnetic structure of La214. D) Magnetic structure of bilayer Y123.

Since HTSC are "real materials" with 3D chemical structures, a coupling J' between adjacent CuO_2 layers needs to be added (Figure 6B). Furthermore, some HTSC contain more than one CuO_2 plane per unit-cell and additional intra-bilayer couplings J_b have to be considered (Figure 6C, Y123 with 2 planes /unit-cell). Finally, if one consider as well the out-of-plane anisotropy α_z, the Hamiltonian takes the complicated form[15,17]:

$$H = J \sum_{n=1,2} \sum_{\langle ij \rangle} \left(S_{in}^x S_{jn}^x + S_{in}^y S_{jn}^y + \alpha_z S_{in}^z S_{jn}^z \right) + J_b \sum_i \mathbf{S}_{i1}\mathbf{S}_{i2} + J' \sum_k \mathbf{S}_{k1}\mathbf{S}_{k2} \qquad (3)$$

where n is the label for two sublattices. A Holstein-Primakoff transformation of the Hamiltonian allows to express the dispersions of the magnons in terms of the exchange parameters J, J_b and J'. In the special case (n=2) where one neglects both the anisotropy (α_z=1) and interlayer components, J'=0 the magnon dispersions are given by:

$$\hbar w^{\pm}(\mathbf{q}) = \sqrt{\left(2J + \frac{J_b}{2}\right)^2 - \left(Jg(\mathbf{q}) \pm \frac{J_b}{2}\right)^2} \qquad (4)$$

where $g(\mathbf{q}) = \cos(q_x a) + \cos(q_y a)$, a being Cu-Cu separation. Both acoustic (+) and optical (-) modes are present (see Figure 7) and can be experimentally distinguished by their relative structure factors along the z-direction. While the acoustic structure factor is proportional to $\sin^2(\pi z Q_l)$ the optical one follows $\cos^2(\pi z Q_l)$. In case one considers as

well interlayer coupling and out-of-plane anisotropy, additional lifting of the degeneracy at low energies can be observed. The parameter J can be directly determined from the slope of the low-energy acoustic branch, while J_b/J, J'/J and α_z can be determined by measuring the spin wave frequencies at zone center and zone boundary (see Figure 7). A careful analysis of the neutron data[17,18] for undoped Y123 yields the following parameters: J˜100-120 meV, J_b/J˜0.02-0.1, J'/J˜$2*10^{-4}$, α_z˜$0.8\text{-}3*10^{-3}$.

Mode n	Zone Center (0,0,0)	Zone boundary (0,0,0.5)
1	0	J'/J
2	a_z/J	$(J'+a_z)/J$
3	$(J'+J_b)/J$	J_b/J
4	$(J'+J_b+a_z)/J$	$(J_b+a_z)/J$

Table 1: Zone center and zone boundary of the square of the magnon frequencies in units of J.

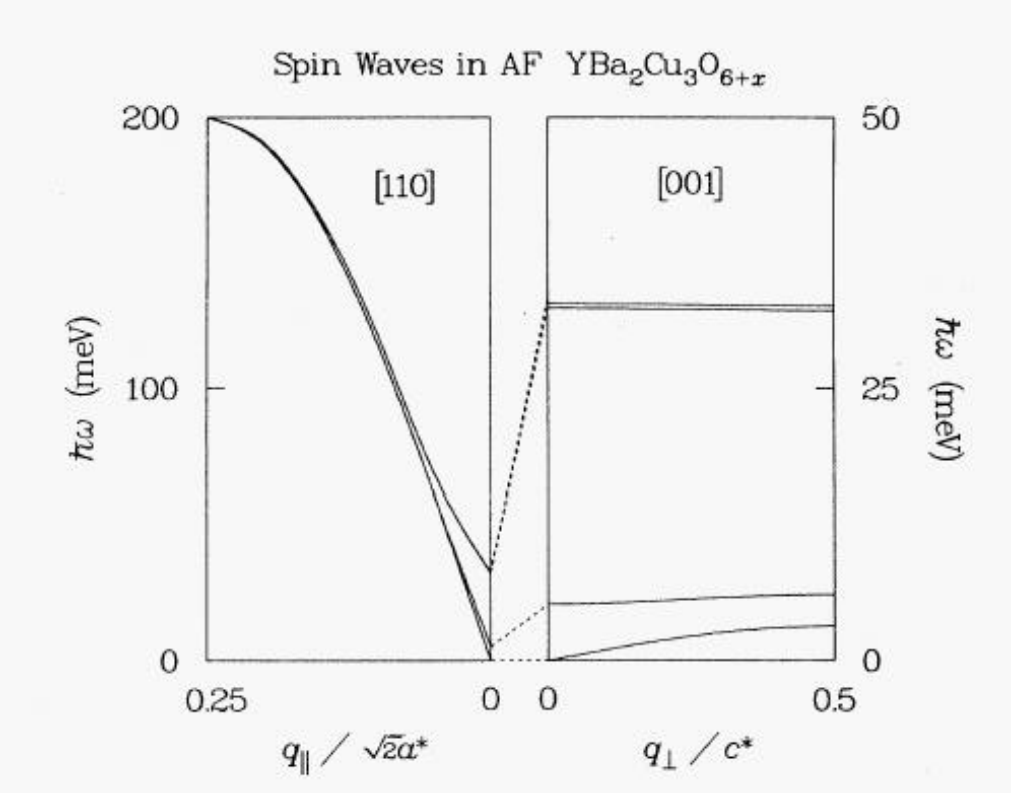

Figure 7:schematic diagram of spin-wave dispersions in Y123 (from Ref. 17).

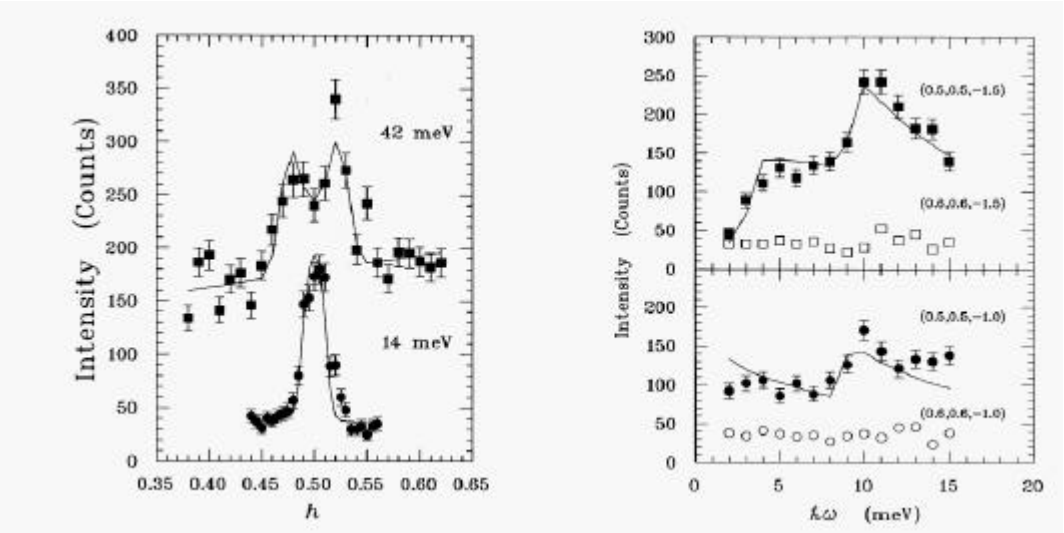

Figure 8: data from Ref. 19 taken at 30 K in Y123 (x=0.15). Left: constant E-scans along (q,q,l_0) showing the large magnon velocity along the (π,π) direction. Right: constant q-scans at the zone center (bottom) and zone boundary (top)**.**

3.3 Superconducting Cuprates

In a simple metal, where the electronic interactions are believed to be weak, one would expect a spin susceptibility with little momentum dependence and extending up to energies defined by the bandwidth t ~ eV and amplitude proportional to $1/t^2$ ~ 1 μ_B^2/eV. In HTSC, many neutron scattering experiments have established the existence of strong (> 100 μ_B^2/eV) antiferromagnetic correlations in both the normal and superconducting states, thus showing the importance of the electronic interactions for the understanding of these materials.

3.3.1 Normal State

While well-defined excitations exist in the undoped AF compound, the situation becomes much more complicated for the doped materials. The cartoon shown in Figure 9 illustrates the main features found around optimal doping. In the *normal state,* some broad excitations exist centered around (π,π). In La214 doped with Sr, these excitations are peaked at some incommensurate wavector $(\pi+\delta,\pi)$[20,21] (See Figure 10). It was furthermore shown that the incommensurability δ increases as a function of increasing doping[22]. Whether some incommensurability also exists in the normal state of Y123 is still debated[23].

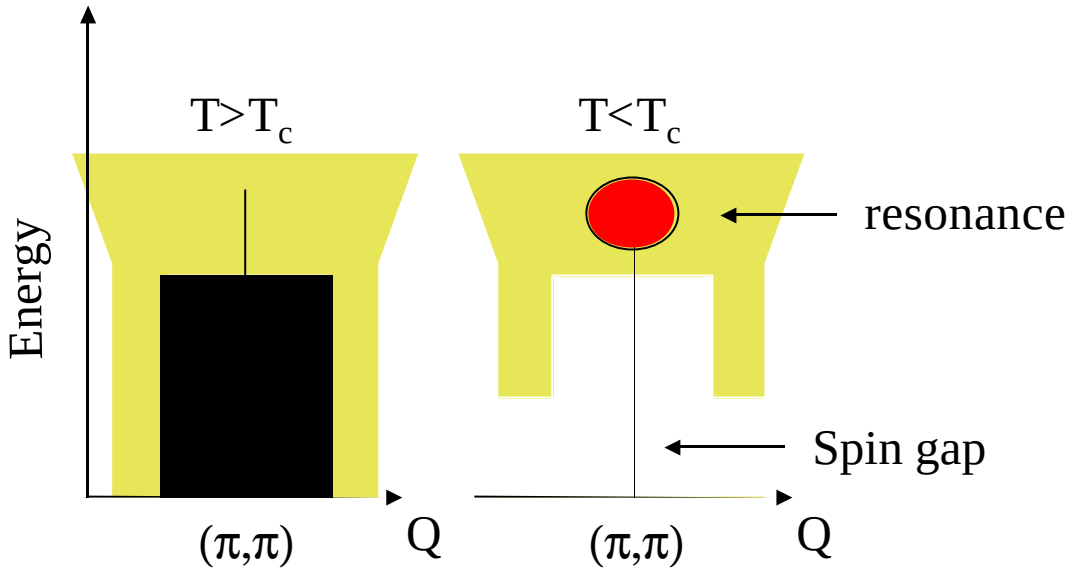

Figure 9: cartoon of the spin excitations in HTSC. Below T_c, a strong renormalization of the spectral weight occurs.

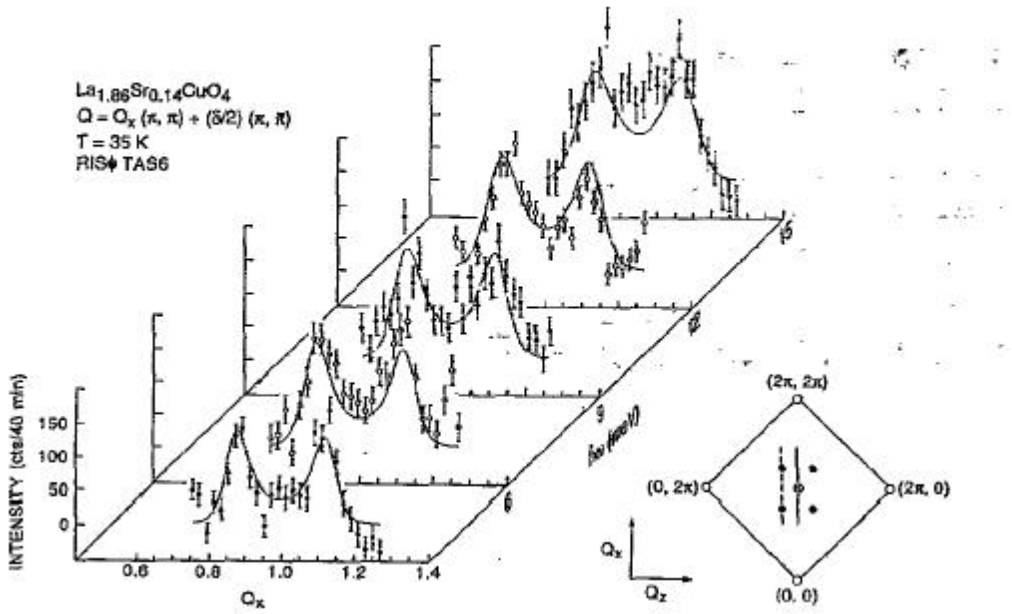

Figure 10: (from Ref. 21) magnetic scattering in the normal state of La(Sr)214 (x=0.14). The Q-cuts are represented by the dashed line in the inset.

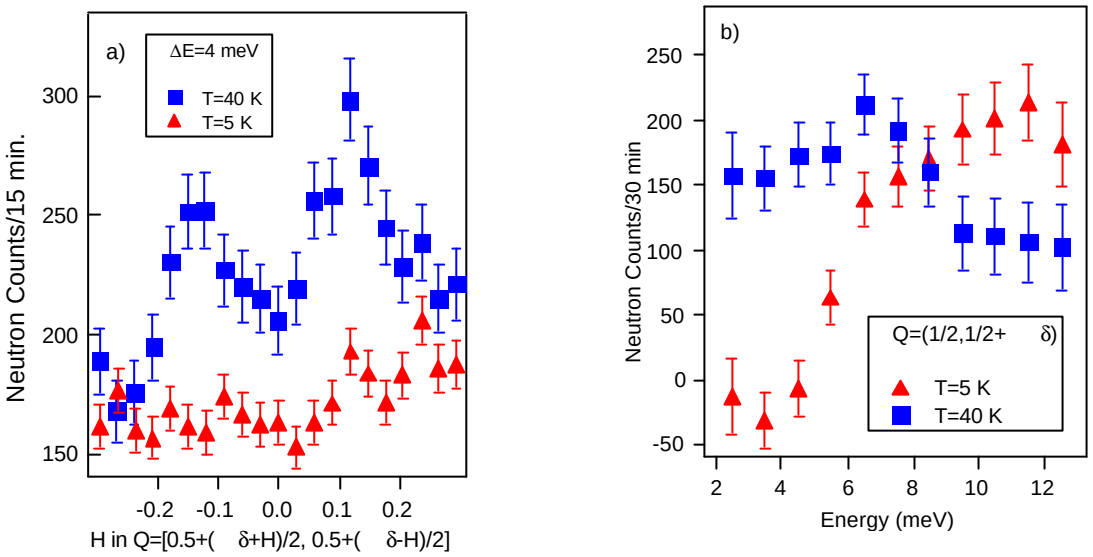

Figure 11: La(Sr)124, x=0.17 a) Q-scans through the incommensurate wavevectors $(\pi+\delta, \pi)$ and $(\pi, \pi+\delta)$ and ?E=4 meV; b) Energy scan at Q=$(\pi+\delta, \pi)$, both in the normal (blue squares) and SC (red triangles) states[24].

3.3.2 superconducting state

The situation changes drastically as one enters the *superconducting state* since a strong renormalization of the spectral weight distribution can be observed, whose two most salient features are:

1) Opening of a spin gap: the observation, in the vicinity of the (π,π) point, of a depletion of the spectral weight at low-energies. This effect was observed both in La124[25] (Figure 11) and Y123[26,27] (Figure 12) compounds.

2) Emergence of a resonance: in those superconductors having the highest T_c's (Y123[26], Bi2212[28]) a strong build up of intensity is observed at energies larger than the spin gap energy (Figure 12).

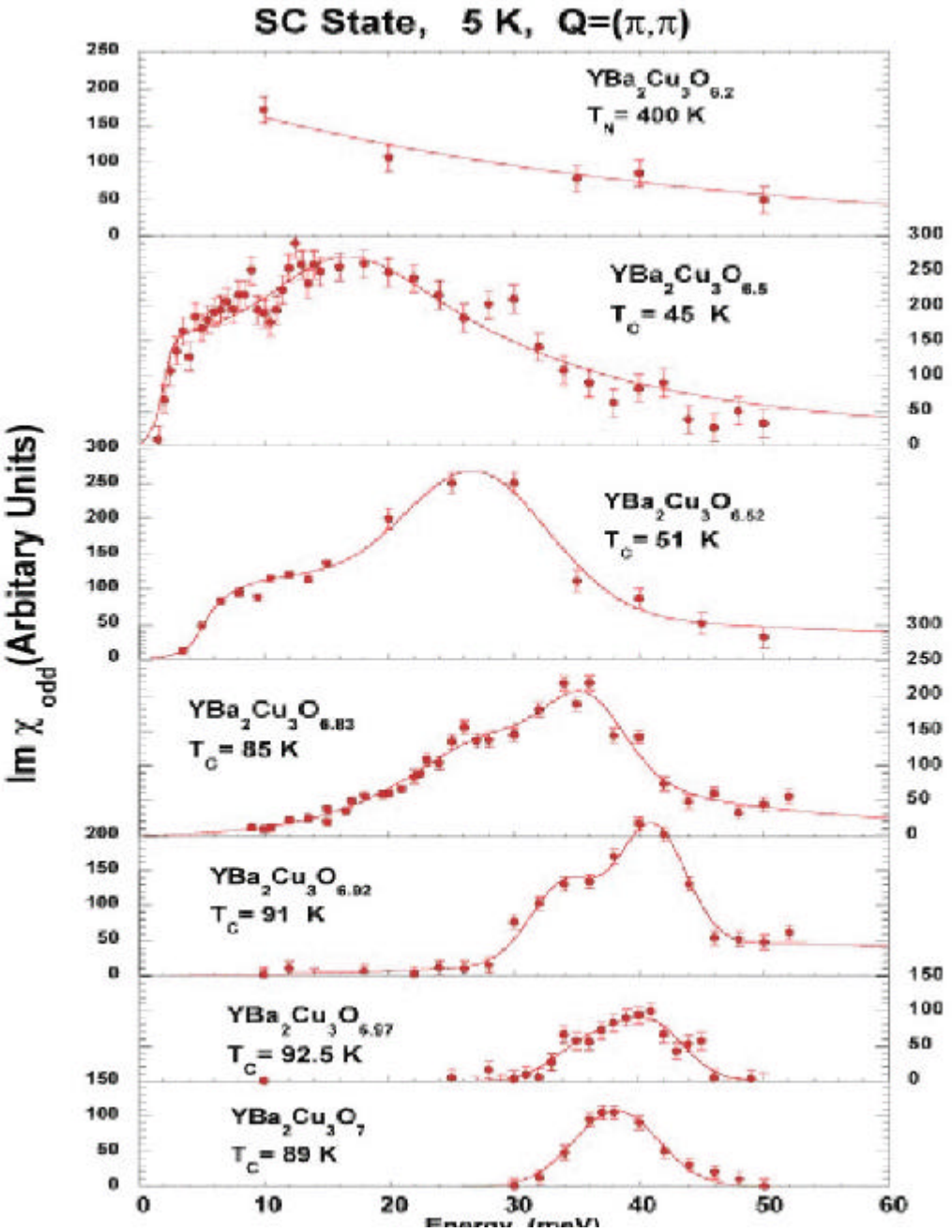
SC State, 5 K, Q=(π,π)
Im χ odd (Arbitary Units)
YBa2Cu3O6.2
TN = 400 K
YBa2Cu3O6.5
TC = 45 K
YBa2Cu3O6.52
TC = 51 K
YBa2Cu3O6.83
TC = 85 K
YBa2Cu3O6.92
TC = 91 K
YBa2Cu3O6.97
TC = 92.5 K
YBa2Cu3O7
TC = 89 K
0
10
20
30
40
50
60

Figure 12: Imaginary part of the odd spin susceptibility at the (π,π) point measured at various doping level in the superconducting state (T=5 K, right panel) (taken from Ref. 27).

3.4 Origin of the spin susceptibility

At optimal doping, both the spin-gap and the resonance vanish above T_c. This fact, together with the observation that the energy of the resonance scales with the superconducting temperature ($E_r \tilde{} 5\ k_B T_c$)[27] indicates that a tight link exists between the magnetic and electronic degrees of freedom in these materials.

Based on itinerant magnetism approaches, many models[29] have been proposed to explain the observed magnetic excitations in HTSC. Basically, these models start from a Fermi liquid picture where the Lindhard Function or non-interacting spin susceptibility c^0 can be written as:

$$c^0(q,w) \approx \sum_k \frac{f_k - f_{k+q}}{\hbar w - (e_{q+k} - e_k) + id} \qquad (5)$$

where e_k and f_k are the electronic band dispersion and Fermi function. In the superconducting phase the Cooper pairs have to be considered and c^0 becomes at T=0[30],

$$c^0(q,w) \approx \sum_k \left[1 - \frac{\Delta_k \Delta_{k+q} + e_k e_{k+q}}{E_k E_{k+q}}\right] \frac{f_k + f_{k+q} - 1}{\hbar w - (E_k + E_{k+q}) + id} \qquad (6)$$

where ?$_k$ and $E_k = \sqrt{e_k^2 + \Delta_k^2}$ are the SC-gap function and quasi-particle energy.

The term in the bracket [] is called the coherence factor and plays a crucial role to explain the existence of spin fluctuations in HTSC. Imagine the following two cases in the limit of ε--> 0:

1) isotropic SC-gap function

?$_k$=|? | --> coherence factor = 0

2) gap function with sign change upon 90 degrees rotation (d-wave)

?$_k$=-?$_{k+(\pi,\pi)}$ --> coherence factor = 2

Within such a Fermionic model, it follows from Eq. 6 that inelastic neutron scattering is also probing, indirectly, the symmetry of the SC-function.

However, the susceptibility as expressed by Eq. 6 is not sufficient to explain the measured inelastic neutron data, since the calculated values are by far too weak. It is therefore necessary to consider an interacting susceptibility, which in an RPA approximation becomes:

$$c(q,w) = \frac{c^0(q,w)}{1 - J(q)\,c^0(q,w)} \qquad (5)$$

where one usually assumes $J(q)=J/2[\cos(q_x a)+\cos(q_y a)]$ to be the superexchange interaction between Cu atoms separated by a distance a.

Within this RPA treatment most features (spin-gap, magnetic resonance and incommensurate excitations) of the measured susceptibility $c''(q,w)$ can be reproduced. Figure 13 shows a calculation by Norman and Pépin[31] based on experimentally determined values of e_k and ?$_k$ by means of ARPES. It should be however mentioned that other scenarios such as those involving the presence of stripes[32] or SO(5) super-symmetry[33] have also been invoked to explain the neutron scattering data.

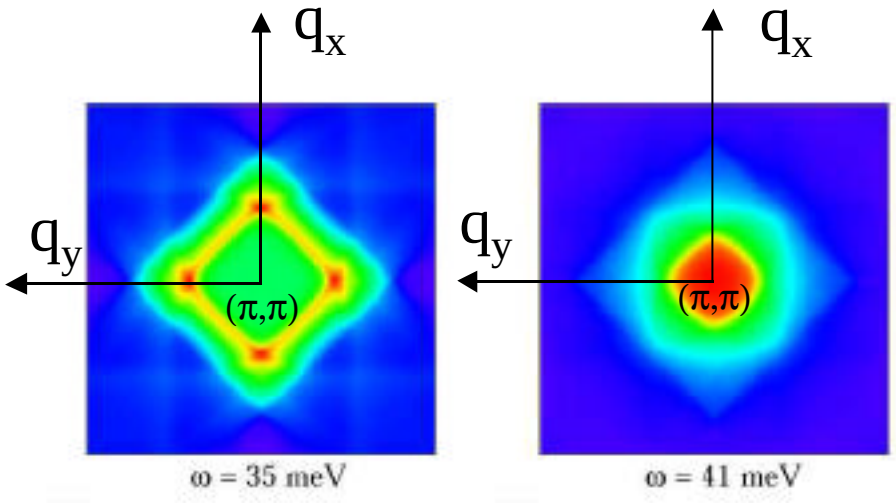

Figure 13: RPA calculation of the dynamic susceptibility at ω=35 meV and 41 meV in the superconducting state of HTSC (from Ref. 31).

3.5 Are the magnetic excitations relevant to SC?

So far we have only established that a tight link exists between the magnetic and electronic degrees of freedom in HTSC. This, however, does not tell us whether the magnetic excitations are relevant or not to superconductivity?

While it was shown that the spin susceptibility can be influenced by the details of the electronic parameters, it has been proposed that the reverse situation is also true[34]: the strong renormalization (through T_c) of the spin susceptibility in the vicinity of the (π,π) point can account for the renormalization of the spectral function at the $(\pi,0)$ point as measured by ARPES (see Figure 14a). Within such an approach the peak-dip-hump structure of the low-temperature spectral function results from the interaction of the electrons with a collective mode (the magnetic resonance?) with the position of the dip corresponding to the sum of both the SC-gap function (?$_0$) and collective-mode (Ω_0) energies (see Figure 14a). It was furthermore shown that the doping dependence of the

energy of the collective mode as inferred from ARPES measurements agrees well with that of the resonance[35]. It remains to understand to what degree this renormalization of the spectral function (via the magnetic resonance) allows a lowering of the total energy of the system and consequently, a stabilization of the superconducting state[36]?

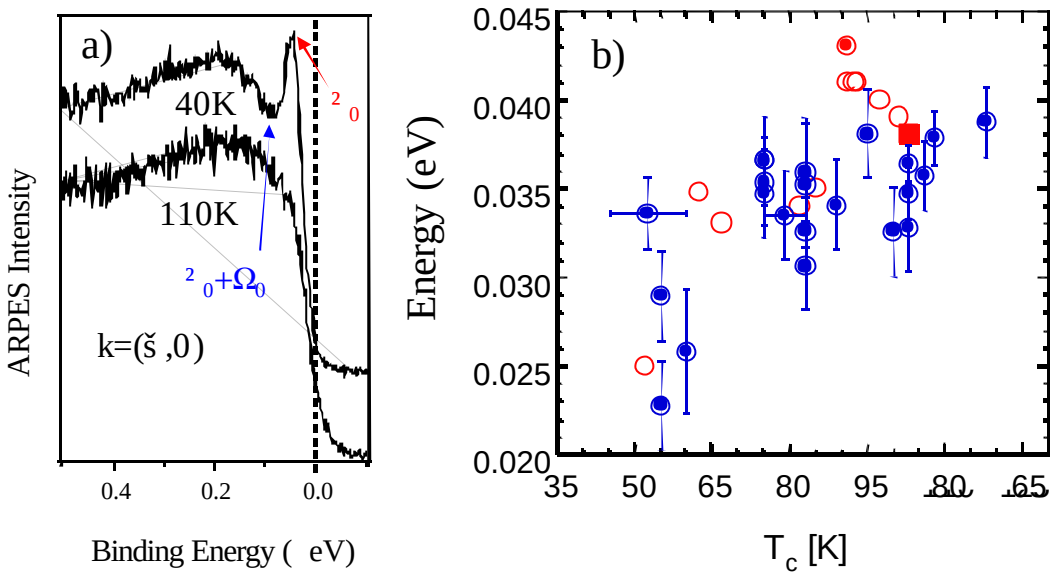

Figure 14: a) ARPES spectra (left) taken at the (π,0) point in the normal (lower) and SC (upper) states of Bi2212 (underdoped T_c=70 K). b) doping dependence of the energy of the collective mode as inferred from ARPES data (blue circles[35]) and from the resonance as inferred from inelastic neutron scattering (empty red circles: YBCO[27]), full red symbols Bi2212[37].

4. <u>The magnetic phase diagram of superconductors</u>

The magnetic phase diagram of type-II superconductors (see Figure 15) can be divided in three main regions: Meissner phase, mixed phase and normal phase. In the Meissner phase, below the lower critical field $H_{c1}(T)$, the magnetic flux is completely excluded from the superconductor, whereas above the upper critical field $H_{c2}(T)$ the normal state is recovered and the magnetic field is homogeneously distributed into the sample. In the mixed phase between $H_{c1}(T)$ and $H_{c2}(T)$ the magnetic flux can penetrate the superconductor in the form of quantized magnetic vortices that interact together and create a vortex lattice (VL). These vortices consist of magnetic flux lines of radius ξ (the coherence length) surrounded by supercurrent screening the external field running over a radius λ? (the London-penetration depth).
Knowing that the magnetic field is confined to flux lines each carrying one flux quantum Φ_o and arranged in a lattice, the symmetry of the VL is found by minimizing the free energy. The result of these calculations for isotropic systems shows that the hexagonal VL rather than the square VL is stabilized[38].

In high-temperature superconductors the situation is complicated because of thermal fluctuations and anisotropy effects[39]. At high temperatures the vortices are thermally activated and the VL can melt into a liquid phase above $H_m(T)$ (see Figure 15). On the other hand a sufficiently large degree of anisotropy can affect the symmetry of the VL. We limit here the discussion to the low temperature part of the phase diagram.

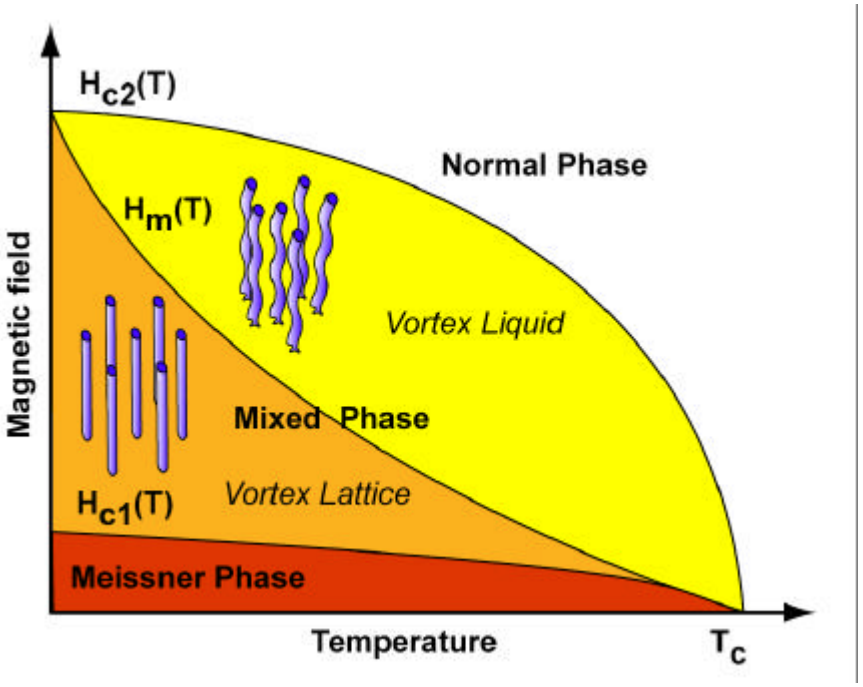

Figure 15: schematic view of the magnetic phase diagram of HTSC.

4. 1 Small Angle Neutron Scattering

The prediction of Abrikosov[1] that quantized magnetic vortices could, under certain circumstances, penetrate the superconductors and build an ordered lattice was confirmed in 1964 by Cribier *et al.*[40] who were able to detect the vortex lattice by neutron scattering experiments. The diffraction of the neutrons by a magnetic vortex lattice occurs because the neutron, due to its magnetic moment, experiences a spatially varying potential. For a square lattice, the spacing of vortex planes $d = \sqrt{\Phi_0 / B}$ (Φ_0 is a flux quantum) is of the order of several 100 Å at 1 Tesla and neutrons having long wavelength (5-20 Å) are required. Since the Bragg condition is fulfilled for angles of the order of a fraction of a degree, small angle scattering (SANS) instruments have to be used. A schematic view of the SANS-I instrument[41] at the Paul Scherrer Institute is displayed in Figure 16.

The neutron intensity being proportional to λ_L^{-4}, SANS observation of the vortex lattice in HTSC (λ_L ~ 1000-2000 Å) is extremely demanding and the first report of a vortex lattice in HTSC was realized by Forgan *et al.*[42] on Y123. In subsequent studies it was shown that at low-fields the lattice has a hexagonal symmetry[43] (Figure 17a). At higher fields, earlier[44] and very recent[45] experiments indicate a transition toward a square VL in Y123.

Due to the extremely large anisotropy a well-defined hexagonal VL in Bi2212 could only be observed at very low fields[46] (see Figure 17b). In La214, it is only very recently that it has been possible to observe a well-defined VL[47]. As shown in Figure 18 the experimental results indicate that, in slightly overdoped La(Sr)214 (x=0.17), a hexagonal pattern exists at low-fields. An intrinsic square vortex lattice (oriented along the Cu-O-Cu bonds) exists at fields larger than 0.4 Tesla. One should notice however that in Y123 the square VL is oriented at 45^0 from the Cu-O-Cu bonds[45].

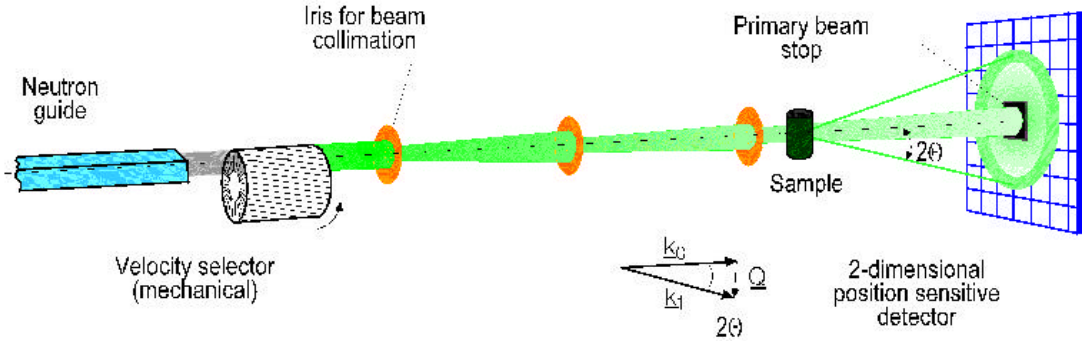

Figure 16: Schematic view of the SANS-I instrument at PSI.

An intrinsic fourfold-symmetry is indicative of the coupling of the VL to some source of anisotropy. Square VL resulting from the anisotropic (d-wave) nature of the superconducting gap via the increasing importance of the anisotropic vortex cores at high fields have been theoretically predicted[48]. In principle other sources of anisotropy, such as those involving Fermi surface/velocity anisotropies[49], dynamical stripes or charge-density waves, could lead to the formation of a square vortex lattice. It remains a challenge to corroborate detailed small angle neutron scattering measurements with other microscopic data in order to explain the origin of this exotic vortex behaviour.

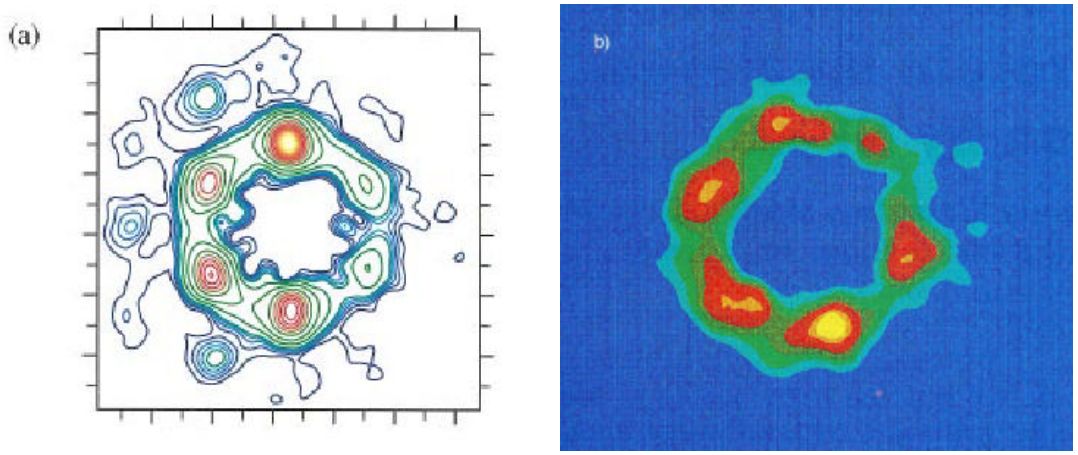

Figure 17: Low-T VL pattern obtained in a) Y123 at 0.2 T with the field applied 33 degrees away from the c-axis[43] and b) in Bi2212[46] at 0.05 T.

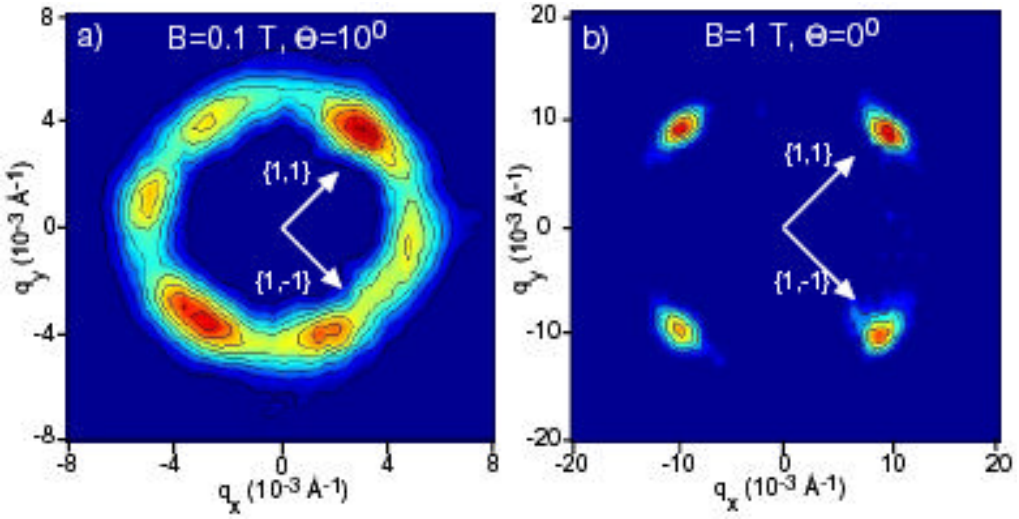

Figure 18: Low-temperature diffraction pattern obtained on La(Sr)214 (x=0.17) at a) B = 0.1 T applied 10 degrees away from the c-axis and at b) B = 1 T applied parallel to the c-axis.

Acknowledgements

I am very grateful to many colleagues, with whom I have collaborated and discussed the topics presented in this lecture. In particular, I would like to thank Ph. Bourges, J. C. Campuzano, R. Cubitt, C. D. Dewhurst, E. M. Forgan, H. M. Fretwell, R. Gilardi, A. Kaminski, S. L. Lee, N. Momono, M. Norman, M. Oda, and M. Randeria.

---

[1] A.A. Abrikosov, Sov. Phys. JETP **5**, 1174-1182 (1957).
[2] J. Bardeen, L. N. Cooper, and J. R. Schrieffer, Phys. Rev. **106**, 162 (1957).
[3] J. M. Ziman, in Principles of the Theory of Solids, Cambridge University Press (1972).
[4] D. R. Tilley and J. Tilley, Superfluidity and Superconductivity, Institute of Physics Publishing (3rd Edition, 1990).
[5] J. G. Bednorz and K. A. Müller, Z. Phys. B condensed Matter **64**, 189 (1986).
[6] P. Coleman, Nature **410,** 320 (2001).
[7] Z. X. Shen *et al*., Phys. Rev. Lett. **70,** 1553 (1993); H. Ding *et al*., Phys. Rev. B **54,** R9678 (1996); J. Mesot *et al*., Phys. Rev. Lett. **83,** 840 (1999).
[8] Tsuei *et al*. Nature **373,** 225 (1995).
[9] For a review see J. L. Tallon and J. W. Loram, cond-mat/0209476 (2002).
[10] J. C. Campuzano *et al*., Phys. Rev. Lett. **64**, 2308 (1990); H. M. Fretwell *et al*., Phys. Rev. Lett. **84**, 4449 (2000); J. Mesot *et al*., Phys. Rev. B **63**, 224516 (2001).
[11] S. Hayden *et al*., Phys. Rev. Lett. **76**, 1344 (1996); H. Mook *et al*., Nature **395**, 580 (1998);
[12] D. Vaknin *et al*., Phys, Rev. Lett. **58,** 2802 (1987); J. M. Tranquada *et al*., Phys, Rev. Lett., **60** 156 (1988); J. Rossat-Mignod *et al.*, Physica C **152,** 19 (1988).
[13] P. Burlet *et al*., Physica C **153-155,** 1115 (1988).

[14] D. Vaknin *et al*., Phys. Rev. B **41**, 1926 (1990)
[15] L. P. Regnault *et al*., in *Neutron Scattering in Layered Copper-Oxide Superconductors*, edited by A. Furrer, Kluwer Academic Publishers, Dordrecht/Boston/London, 1998.
[16] S. M. Hayden, in *Neutron Scattering in Layered Copper-Oxide Superconductors*, edited by A. Furrer, Kluwer Academic Publishers, Dordrecht/Boston/London, 1998, pp 135.
[17] J. M. Tranquada *et al*., Phys. Rev. B. **40**, 4503 (1989).
[18] D. Reznick *et al*., Phys. Rev. B. 53, R14741 (1996); S. M. Hayden *et al*., Phys. Rev. B. 54, R6905 (1996);
[19] S. Shamoto *et al*., Phys. Rev. B. **48**, 13817 (1993).
[20] T. R. Thurston *et al*., Phys. Rev B **40**, 4585 (1989).
[21] T. E. Mason *et al*., Phys. Rev. Lett. **68**, 1414 (1992); T. R. Thurston *et al*., Phys. Rev. B **46**, 9128 (1992).
[22] S.-W. Cheong *et al*., Phys. Rev. Lett. **67**, 1791 (1991); K. Yamada *et al*., Phys. Rev. B **57**, 6615 (1998);
[23] H. A. Mook *et al.*, *Nature* **395**, 580 (1998); Ph. Bourges *et al*., Science **288**, 1234 (2000).
[24] R. Gilardi *et al*., submitted.
[25] G. Aeppli *et al*., Science **278**, 1432 (1997); for a review see M. A. Kastner *et al*., Rev. Mod. Phys. **70**, 897 (1998).
[26] J. Rossat-Mignot *et al*., Physica C 185-189, 86 (1991).
[27] for a review see Ph. Bourges, in *The Gap Symmetry and Fluctuations in High-Temperature Superconductors*, Edited by J. Bok, G. Deutscher, D. Pavuna and S. A. Wolf (Plenum Press, 1988) (cond-mat/9901333).
[28] H. F. Fong *et al.*, Nature **398**, 588 (1999).
[29] J. P. Lu, Phys. Rev. Lett. **68**, 125 (1992); Y. Ohashi and H. Shiba, J. Phys. Soc. Jpn. **62**, 2783 (1993); A. J. Millis and H. Monien, Phys. Rev. B **54**, 16172 (1996); P. Monthoux and D. J. Scalapino, Phys. Rev. Lett. **72**, 1874 (1994); M. Lavagna and G. Stemmann, Phys. Rev. B **49**, 4235 (1994); G. Blumberg *et al*., Phys. Rev. B **52**, R15741 (1995); F. Onufrieva and J. Rossat-Mignod, Phys. Rev. B **52**, 7572 (1995); D. Z. Liu *et al*., Phys. Rev. Lett. **75**, 4130 (1995); I. I. Mazin and V. m. Yakovenko, Phys. Rev. Lett. **75**, 4134 (1995); L.Yin *et al*; Phys. Rev. Lett. **78**, 3559 (1997). M. R. Norman, Phys. Rev. B **61**, 14 751 (2000).
[30] J. R. Schrieffer, in *Theory of Superconductivity* (Frontiers in Physics (20), Addison Wesley) (1988).
[31] M. R. Norman and C. Pépin, to appear in Rev. Prog. Phys., cond-mat/0302347
[32] S. A. Kivelson, E. Fradkin, and V. J. Emery, Nature **393**, 550 (1998).
[33] S. C. Zhang, Science, **275** 1089 (1997).
[34] M. R. Norman *et al*., Phys. Rev. Lett. **79**, 3506 (1997); A. Abanov and A. V. Chubukov, Phys. Rev. Lett. **83**, 1652 (1999).
[35] J. C. Campuzano *et al*., Phys. Rev. Lett. **83**, 3709 (1999).
[36] M. R. Norman *et al*., Phys. Rev. B **61**, 14742 (2000).
[37] H. F. Fong *et al.*, Nature **398**, 588 (1999); H. A. Mook, F. Dogan, and B. C. Chakoumakos, cond-mat/9811100; H. He *et al*., Phys. Rev. Lett. **86**, 1610 (2001).
[38] W.H. Kleiner *et al*., Phys. Rev. **133,** A1226 (1963).

[39] G. Blatter *et al*., Rev. Mod. Phys. **66**, 1125 (1994).
[40] D. Cribier *et al*., Phys. Lett. **9**, 106 (1964).
[41] More information about the SANS instrument at PSI can be obtained on the web: http://sans.web.psi.ch/
[42] E. M. Forgan *et al*., Nature **735**, 343 (1990).
[43] S. T. Johnson *et al*., Phys. Rev. Lett. **82**, 2792 (1999);
[44] B. Keimer *et al.*, Science **262**, 83 (1993).
[45] S. Brown *et al*., private publication.
[46] R. Cubitt *et al.*, Nature **365**, 407 (1993).
[47] R. Gilardi *et al*., Phys. Rev. Lett. **88**, 217003 (2002).
[48] A.J. Berlinsky *et al*., Phys. Rev. Lett. 75 (1995) 2200; M. Ichioka *et al*., Phys. Rev. B 59 (1999) 8902
[49] N. Nakai *et al.*, Phys. Rev. Lett. **89**, 237004 (2002)